JOURNAL OF MATERIALS SCIENCE 29 (1994) 5725–5731

Residual stress-induced spontaneous microcracking in α-SiC platelet Al_2O_3 composites

Y.-S. CHOU, D. J. GREEN
Department of Materials Science and Engineering, The Pennsylvania State University, University Park, PA 16802, USA

The micromechanical stresses associated with hexagonal (6H) α-SiC platelets within a fine-grained alumina matrix were calculated using an Eshelby approach. The stresses within and around the interface of SiC platelets were determined. Both stresses were found to be strongly dependent on the morphology and the volume fraction of the SiC particles. The morphology effect, however, tended to be limited at aspect ratios $\geqslant 10$. Owing to anisotropy in the thermal and elastic properties of α-SiC, the residual stresses just outside the inclusion also depended on the position along the SiC/Al_2O_3 interfaces. The maximum tensile stress was found at the edges of SiC platelets. There were two principal tangential tensile stresses which differed greatly at the edges of disc-shaped inclusions. The results of the stress analysis were consistent with observed differences in microcrack morphology and the resultant reduction of the Young's modulus of the composites.

1. Introduction

Studies of whisker-reinforced ceramics have shown substantial improvements in fracture toughness and resistance to slow crack growth via the incorporation of strong, small-diameter whiskers into ceramic matrices [1, 2]. However, the improvements are often overshadowed by the hazardous nature [1] of the fine whiskers and the constraint produced by the reinforcement that inhibits densification [3, 4]. Recently, an alternative to whisker reinforcement, i.e. platelet reinforcement, has been explored. Ceramic, single-crystal platelets, e.g. SiC [5, 6], Al_2O_3 [7], and ZrB_2 [8] have been developed and employed to make ceramic- and metal-matrix composites. The toughening effect of platelets in ceramic-matrix composites was found to be quite encouraging, e.g. a K_{Ic} value of 7.1 MPa $m^{1/2}$ was reported for an Al_2O_3 composite containing 30 vol % SiC platelets [9]. The use of large SiC platelets in an alumina matrix, however, in certain conditions can degrade the mechanical properties. For example, the Young's modulus and the fracture toughness of the composites were greatly reduced by the occurrence of spontaneous microcracking. The cause of these microcracks was considered to be a result of the residual stresses from thermal expansion mismatch between SiC and Al_2O_3.

The residual stresses in SiC whiskers/Al_2O_3 composites have been studied [10–14]. However, in these analyses, the silicon carbide particles or whiskers were cubic (3C), which is not the case in the current system, in which single-crystal hexagonal (6H) SiC platelets were used. The single-crystal elastic properties of the hexagonal (6H) α-SiC polytype and the cubic (3C) β polytype are similar in magnitude [15, 16], but the thermal expansion anisotropies of these materials are different [17]. In this paper, the micromechanical stresses associated with hexagonal α-SiC platelets within a fine-grained polycrystalline alumina matrix have been calculated. The effects of the aspect ratio and the volume fraction of a SiC platelet were investigated. In addition, microstructural observations of a SiC platelet/Al_2O_3 composite containing spontaneous microcracking are presented. The different microcrack morphologies and their relationship to the residual stresses are discussed.

2. Micromechanical stress calculations

The analysis used to calculate the micromechanical stresses is based on studies by Eshelby [18] and Mori and Tanaka [19]. Eshelby in 1957 analysed the stress state of an ellipsoidal inclusion in an infinite matrix. The stress fields inside the inclusion and around its interface were obtained. Mori and Tanaka later modified Eshelby's model to account for the problem of finite concentration of inclusions. In their studies, however, the strain due to thermal expansion mismatch between matrix and inclusions was not included. In this paper, the thermal strain will be incorporated and both analytical approaches are described briefly below.

Consider the model, shown in Fig. 1, in which the SiC ellipsoidal inclusions are aligned along X_1, X_2, and X_3 axes. The axes are chosen such that X_1 and X_2 are parallel to the crystallographic $\langle 2\bar{1}\bar{1}0\rangle$ and X_3 parallel to $\langle 0001\rangle$. The ellipsoidal α-SiC (6H) single-crystal inclusions are represented by two geometrical parameters, L and d, where L is specified as parallel to X_3 and d is parallel to X_1 and X_2. The inclusions and the matrix are assumed perfectly bonded, and with the

0022–2461

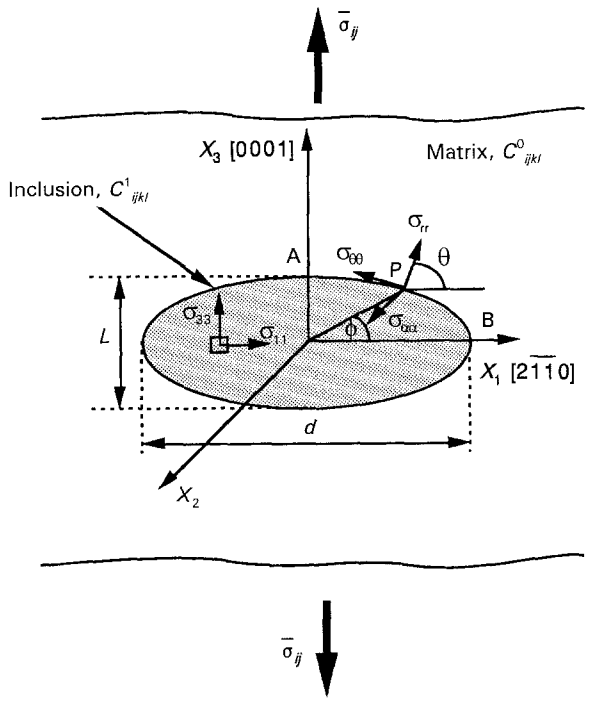

Figure 1 Single-crystal ellipsoidal SiC (6H) particle in an isotropic alumina matrix.

elastic stiffness constants, C^1_{ijkl} and C^0_{ijkl}, respectively. To give the platelet morphology, the inclusion geometry is considered to be axisymmetric around X_3, giving the "disc-like" morphology. Based on the Eshelby method, the stress within a single-crystal particle in an infinite matrix, $\sigma^{(in)}_{ij}$, when subjected to an eigenstrain such as a thermal strain, ε^t_{kl}, can be expressed as

$$\begin{aligned}\sigma^{(in)}_{ij} &= \bar{\sigma}_{ij} + \sigma^{pt}_{ij} \\ &= C^1_{ijkl}(\varepsilon^0_{kl} + \varepsilon^{pt}_{kl} - \varepsilon^t_{kl}) \\ &= C^0_{ijkl}(\varepsilon^0_{kl} + \varepsilon^{pt}_{kl} - \varepsilon^*_{kl}) \end{aligned} \quad (1)$$

where ε^0_{kl} is the strain due to the applied stress, $\bar{\sigma}_{ij}$. These two tensors are related by

$$\bar{\sigma}_{ij} = C^0_{ijkl}\varepsilon^0_{kl} \quad (2)$$

The thermal strain, due to the strong temperature dependence of α [17], is calculated as

$$\varepsilon^t_{kl} = \int_{T_1}^{T_2} [\alpha^1_{kl}(T) - \bar{\alpha}^\circ(T)]dT \quad (3)$$

where T_2 is the temperature below which the complete stress relaxation by "creep"-related processes can be neglected (a temperature of 1300 °C was assumed), T_1 is room temperature, α^1_{kl} are the thermal expansion coefficients of α-SiC, and $\bar{\alpha}^\circ$ is the average thermal expansion coefficient of the matrix. The ε^{pt}_{kl} and σ^{pt}_{ij} are the disturbances of the strain and stress due to the presence of the second-phase particle, and the ε^*_{kl} is the equivalent eigenstrain of the inclusion, introduced into the region of the matrix, to account for the effect of its elastic inhomogeneity.

Eshelby's solution readily provides the relation

$$\varepsilon^{pt}_{kl} = S_{klmn}\varepsilon^*_{mn} \quad (4)$$

where S_{klmn} is the transformation tensor, which is dependent on the Poisson's ratio of the matrix and the aspect ratio of the inclusions.

At a finite concentration of inclusions, the stress in the inclusion can be calculated by the method of Mori and Tanaka [19] as

$$\begin{aligned}\sigma^{(in)}_{ij} &= \bar{\sigma}_{ij} + \tilde{\sigma}_{ij} + \sigma^{pt}_{ij} \\ &= C^1_{ijkl}(\varepsilon^0_{kl} + \tilde{\varepsilon}_{kl} + \varepsilon^{pt}_{kl} - \varepsilon^t_{kl}) \\ &= C^0_{ijkl}(\varepsilon^0_{kl} + \tilde{\varepsilon}_{kl} + \varepsilon^{pt}_{kl} - \varepsilon^*_{kl}) \end{aligned} \quad (5)$$

where $\tilde{\sigma}_{ij}$ and $\tilde{\varepsilon}_{kl}$ are the differences between finite concentrations and single inclusion for the average stress and strain in the matrix, respectively. Because volume average of the mean stresses in the matrix and the inclusions must be in balance with $\bar{\sigma}_{ij}$, we have

$$\tilde{\sigma}_{ij} = -V\sigma^{pt}_{ij} \quad (6)$$

where V is the volume fraction of inclusions. The average perturbed strain in the matrix is

$$\tilde{\varepsilon}_{ij} = -V(S_{ijkl} - I_{ijkl})\varepsilon^*_{kl} \quad (7)$$

where I_{ijkl} is the fourth-rank identity tensor. With Equations 7 and 4, ε^*_{kl} may be readily solved by substituting into Equation 5 and the stresses inside the inclusion can be rewritten as

$$\sigma^{(in)}_{ij} = C^0_{ijkl}[\varepsilon^0_{kl} + (1 - V)(S_{klmn} - I_{klmn})\varepsilon^*_{mn}] \quad (8)$$

The micromechanical stresses within the matrix just outside the inclusion, $\sigma^{(out)}_{ij}$, have been suggested by Mura and Cheng [20] as

$$\sigma^{(out)}_{ij} = \sigma^{(in)}_{ij} + C^0_{ijkl}[-C^0_{pqmn}\varepsilon^*_{mn}M_{kp}n_q n_l + \varepsilon^*_{kl}] \quad (9)$$

where

$$M_{kp} = \frac{1}{\mu_0}\left[\delta_{kp} - \frac{n_k n_p}{2(1 - \upsilon_0)}\right] \quad (10)$$

and n_i is the unit outward normal of the inclusion, δ_{kp} the Kronecker delta, and μ_0 and υ_0 the shear modulus and Poisson's ratio of the matrix, respectively.

Applying Equations 8–10, the residual stresses of an ellipsoidal inclusion with an oblate shape or other shapes such as whiskers and spheres, can be obtained as long as the matrix is assumed to be isotropic in both thermal expansion and elastic properties. However, the eigenstrains, ε^*_{ij}, in actual applications of the theory may be very difficult to obtain from Equation 8. A matrix method has been suggested by Li and Bradt [10, 21, 22] to simplify the above equations and is used in this paper.

3. Residual stresses within the α-SiC inclusion

The elastic stiffness data of α-SiC [15] and Al_2O_3 used for the calculation are listed in Table I. (The stiffness data for Al_2O_3 are calculated from the single-crystal compliance data [23] assuming that the fine-grained polycrystalline Al_2O_3 matrix is isotropic.) Here, we use the room-temperature values for simplification, because the elastic constants of SiC and Al_2O_3 are only slightly temperature dependent. Instead of using

TABLE I Elastic stiffness data of α-SiC and Al_2O_3

Material	Stiffness (GPa)				
	C_{11}	C_{12}	C_{13}	C_{33}	C_{44}
α-SiC	479	98	56	521	148
Al_2O_3	468	142	142	163	163

TABLE II Thermal expansion coefficients of α-SiC and Al_2O_3 as a function of temperature

Material	Equations for α_{ij} or $\bar{\alpha}^0$
α-SiC	$\alpha_{11} = 3.27\times10^{-6} + 3.25\times10^{-9}\,T - 1.36\times10^{-12}\,T^2$ ($°C^{-1}$)
	$\alpha_{33} = 3.18\times10^{-6} + 2.48\times10^{-9}\,T - 8.51\times10^{-13}\,T^2$ ($°C^{-1}$)
Al_2O_3	$\bar{\alpha}^0 = 5.84\times10^{-6} + 7.88\times10^{-9}\,T - 4.69\times10^{-12}\,T^2$ ($°C^{-1}$)

the room-temperature values, thermal expansion coefficients as a function of temperature are used. Table II lists the equations of these coefficients for α-SiC [17] and the alumina matrix (the function for alumina is obtained by a least-square fitting of raw thermal expansion data [24]).

The residual stresses within an oblate ellipsoidal α-SiC particle, $\sigma_{11}^{(in)}$ and $\sigma_{33}^{(in)}$, are plotted in Figs 2 and 3 respectively, as they vary with the aspect ratio and the volume fraction. As the elastic and thermal expansion properties are equal along X_2 and X_1 directions, the residual stress along the X_2 direction, $(\sigma_{22}^{(in)})$, is found to be equal to that along X_1 axis, $(\sigma_{11}^{(in)})$. Indeed, as the basal plane is isotropic with respect to thermal expansion and elastic constants, the stresses are independent of orientation in the X_1–X_2 plane. From these figures, the residual stresses within an oblate ellipsoidal α-SiC particle are all compressive, which is quite obvious, because the thermal expansion of the matrix is much larger than the inclusions. In addition, the stresses are highly dependent on the aspect ratio or the shape of the inclusion. For example, $\sigma_{11}^{(in)}$ of a composite ($V = 0$) decreases from -1.56 GPa to -2.41 GPa for a change of aspect ratio from 1 to 10, i.e. from a sphere to a disc-like particle. The stress decreases with the increasing aspect ratio. For $\sigma_{33}^{(in)}$, the trend is reversed, i.e. the stress increases with the increasing aspect ratio. For example, $\sigma_{33}^{(in)}$ of a composite ($V \approx 0$) increases from -1.64 GPa to -0.32 GPa for an aspect ratio change from 1 to 10. Both $\sigma_{11}^{(in)}$ and $\sigma_{33}^{(in)}$ reach a plateau value at aspect ratio ≈ 10 (from this value the stresses only change a few per cent as the aspect ratio approaches infinity).

The effect of volume fraction on residual stresses inside α-SiC particles, however, shows the same dependence for both $\sigma_{11}^{(in)}$ and $\sigma_{33}^{(in)}$, i.e. both stresses increase with increasing SiC volume fraction. For example, $\sigma_{11}^{(in)}$ of an SiC inclusion with an aspect ratio of 10 increases from -2.41 GPa to -1.67 GPa as the volume fraction changes from 0 to 0.3, and $\sigma_{33}^{(in)}$ increases from -0.32 GPa to -0.23 GPa for the same volume fraction change.

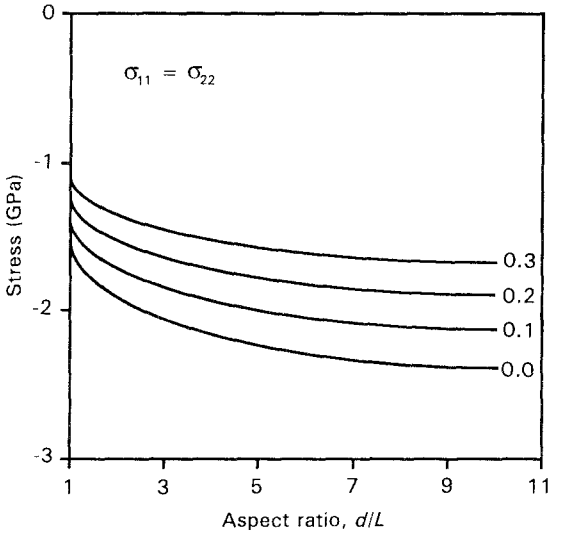

Figure 2 Residual stresses, $\sigma_{11}^{(in)}$ and $\sigma_{22}^{(in)}$, within an α-SiC ellipsoidal particle as a function of aspect ratio and volume fraction (numbers shown).

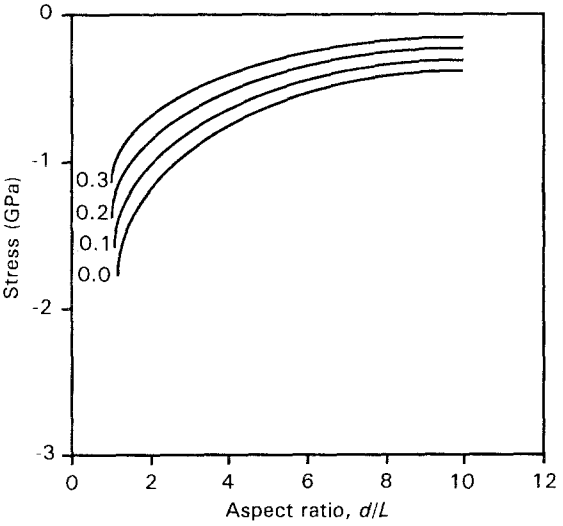

Figure 3 Residual stress, $\sigma_{33}^{(in)}$, within an α-SiC ellipsoidal particle as a function of aspect ratio and volume fraction (numbers shown).

4. Residual stresses within the Al_2O_3 matrix

The stresses in the matrix just outside the inclusion are also of interest and can be readily calculated. For convenience, the radial, σ_{rr}, and tangential, $\sigma_{\theta\theta}$ and $\sigma_{\alpha\alpha}$, components of the stresses are determined. As mentioned in the previous section, the inclusion is isotropic with respect to both thermal expansion and elastic constants in the basal plane; therefore, the stresses just outside the inclusion are also independent of orientation in the X_1–X_2 plane. For convenience, we only consider the stresses at the perimeter of inclusion on the X_1–X_3 plane from point A to point B. For this case, the directions of σ_{rr} and $\sigma_{\theta\theta}$ are in the X_1–X_3 plane and $\sigma_{\alpha\alpha}$ is parallel to X_2 (see Fig. 1). For other planes containing the X_3 axis, $\sigma_{\alpha\alpha}$ will no longer be parallel to X_2; however, its magnitude remains the same. Once the principal stresses, $\sigma_{11}^{(out)}$, $\sigma_{22}^{(out)}$, and $\sigma_{33}^{(out)}$, at a point P in the X_1–X_3

plane are determined, the radial and tangential stresses are given as

$$\sigma_{rr} = \sigma_{11}^{(out)} \cos^2\theta + \sigma_{33}^{(out)} \sin^2\theta \quad (11)$$

$$\sigma_{\theta\theta} = \sigma_{11}^{(out)} \sin^2\theta + \sigma_{33}^{(out)} \cos^2\theta \quad (12)$$

$$\sigma_{\alpha\alpha} = \sigma_{22}^{(out)} \quad (13)$$

where θ is the angle characterizing the unit normal and can be related to angle ϕ (see Fig. 1) through the geometrical relationship [25]

$$\tan\phi = \delta^2 \tan\theta \quad (14)$$

where δ ($= d/L$) is the aspect ratio of the inclusion.

Figs 4–6 show the stresses just outside the inclusion, σ_{rr}, $\sigma_{\theta\theta}$ and $\sigma_{\alpha\alpha}$, as a function of angle, ϕ, and volume fraction of SiC oblate particles with an aspect ratio of 10, respectively. Contrary to residual stresses inside the α-SiC inclusions, which are hydrostatic, the stresses just outside the inclusions are not hydrostatic but depend on location along the interface (angle ϕ). However, the dependences are very limited, i.e. all the stresses reach some plateau values at angle $\phi \geqslant 10°$. As for the effect of SiC volume fraction, it is clear that σ_{rr}, which is compressive, shows a lower dependence on volume fraction than $\sigma_{\theta\theta}$ and $\sigma_{\alpha\alpha}$, which are tensile in nature. Both $\sigma_{\theta\theta}$ and $\sigma_{\alpha\alpha}$ increase with increasing SiC volume fraction. This trend, the residual tensile stresses in the matrix increasing with increasing SiC volume fractions, has been proven experimentally by Majumdar and Kupperman [12] and Abuhasan *et al.* [13] using neutron and X-ray diffraction in SiC whisker/Al_2O_3 composites. It is also interesting to note that the two types of tangential tensile stresses, $\sigma_{\theta\theta}$ and $\sigma_{\alpha\alpha}$, are not equal at low angles ($\phi \leqslant 10°$), i.e. $\sigma_{\theta\theta}$ is much greater than $\sigma_{\alpha\alpha}$. For example, $\sigma_{\theta\theta}$ is 1.97 GPa and $\sigma_{\alpha\alpha}$ is only 0.82 GPa of a composite ($V = 0.3$) containing SiC inclusions with an aspect ratio of 10. At higher angles ($\phi \geqslant 10°$), the two become equal (see Figs 5 and 6). Similar results that the extreme stresses exist at either point A ($\phi = 90°$) or B ($\phi = 0°$) have been reported by Li and Bradt [10] in SiC(3C)/alumina composites.

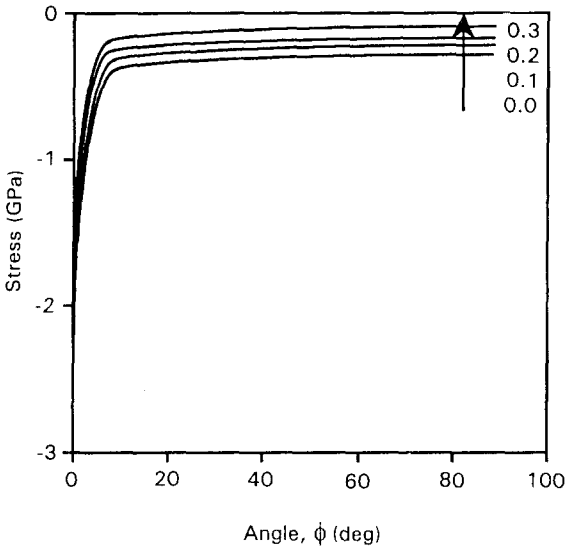

Figure 4 Radial stress, σ_{rr}, around a α-SiC ellipsoidal particle (aspect ratio = 10) in the alumina matrix for different angle, ϕ, (numbers inside the graph represent the volume fraction).

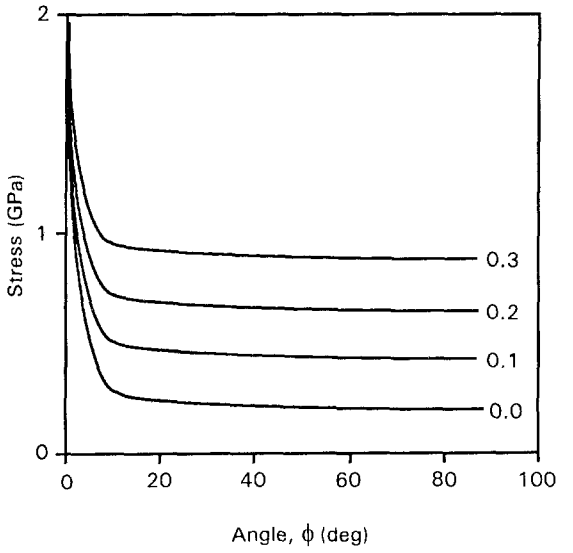

Figure 5 Tangential stress, $\sigma_{\theta\theta}$, around a α-SiC ellipsoidal particle (aspect ratio = 10) in the alumina matrix for different angle, ϕ, (numbers inside the graph represent the volume fraction).

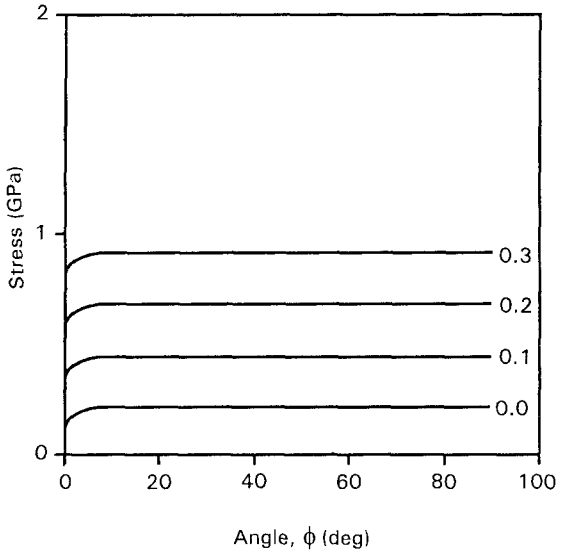

Figure 6 Tangential stress, $\sigma_{\alpha\alpha}$, which is parallel to X_2 axis, around a α-SiC ellipsoidal particle (aspect ratio = 10) in the alumina matrix for different angle (ϕ) (numbers inside the graph represent the volume fraction).

5. Microstructural observation in SiC platelet/Al_2O_3 composites

From the previous section, it is clear that very high tensile stresses exist just outside the inclusion particularly at location B (Fig. 1) and they increase with increasing SiC volume fraction. Consequently, one would expect that radial microcracks could form at this location in SiC/Al_2O_3 composites. Indeed, radial microcracks have been observed by Chou and Green [9] in an SiC platelet/Al_2O_3 composite. Similar radial microcracks have been found by Davidge and Green [26] in two-phase ceramic/glass materials, in which the ceramic inclusion also has a smaller coefficient of thermal expansion than the glass matrix.

For composites containing plate-like inclusions, one would expect cracks to initiate at the edges of the platelets, where the tensile stresses are maximum (Fig. 5). For a platelet composite, it needs also to be realized that these radial cracks could exist with various morphologies as compared to the radial microcracks found in composites containing spherical particles. For example, the fracture surface of the radial cracks could be perpendicular or parallel to the platelet faces and these will be referred to as Type I and II microcracks, respectively, whereas the radial cracks would be perpendicular to the surface of spheres in the composites containing such particles. For the latter case, such morphologies were observed by Davidge and Green for ThO_2 spheres in glass [26]. Both Type I and II radial microcracks were observed in some preliminary studies of a SiC ($V = 0.1$)/Al_2O_3 composite using large SiC platelets ($\sim$ 48 μm, aspect ratio $\sim$ 8). A typical example is shown in Fig. 7. Large radial microcracks with lengths in the range of 100 μm are clearly seen in the optimal micrograph (Type I). In addition, smaller scale radial microcracks with crack planes approximately parallel to the platelet faces are also present at the circumference of SiC platelets (Type II, shown by the arrows). It should be noted that the microcracks observed here may not be exactly perpendicular or parallel to platelet faces but rather deviate by some angles, because the stress state at the edge of the platelet contains biaxial tensile components, although the magnitudes of stresses, $\sigma_{\theta\theta}$ and $\sigma_{\alpha\alpha}$, are not equal to low ϕ angles.

The occurrence of Type II microcracks is expected because the tangential tensile stress, $\sigma_{\theta\theta}$, is found to be the highest stress. For the case of a SiC volume fraction of 0.1 and an aspect ratio of 8, $\sigma_{\theta\theta}$ at the platelet edges is 1.73 GPa which is much larger than $\sigma_{\alpha\alpha}$ of 0.36 GPa. Even though $\sigma_{\alpha\alpha}$ is less than $\sigma_{\theta\theta}$ these stresses must be responsible for the Type I microcracks. Because the size of SiC platelets is reduced, however, the formation of Type I microcracks becomes limited. Fig. 8 shows the microstructure of a SiC ($V = 0.2$)/Al_2O_3 composite using a smaller platelets ($\sim$ 24 μm) and aspect ratio ($\sim$ 4). It is clear that only Type II microcracks are present. The stresses at the platelet edges calculated for this case are 1.70 and 0.76 GPa for $\sigma_{\theta\theta}$ and $\sigma_{\alpha\alpha}$, respectively. The tangential stress, $\sigma_{\alpha\alpha}$, is about twice as large as that in the composites with larger platelets and yet no Type I microcracks are found. The formation of Type I cracks is, therefore, believed to be associated with the size of the SiC platelets used. A critical size effect, such that microcracking does not occur for inclusions below a given size, is an established phenomenon in brittle particulate composites [27].

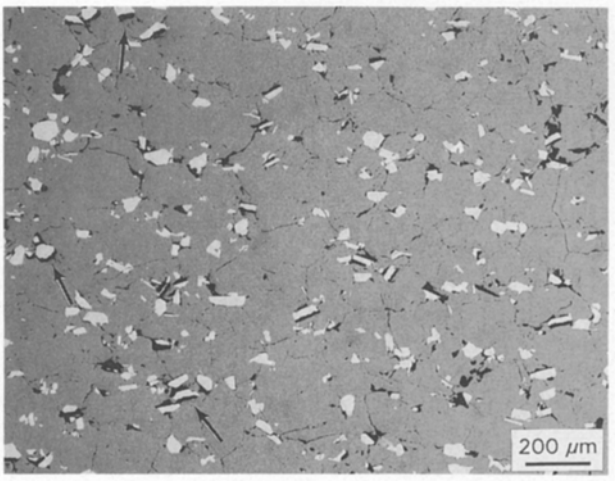

Figure 7 Spontaneous microcracking in SiC-platelet/Al_2O_3 composites ($V = 0.1$) using large size ($\sim$48 μm) platelets. Note there are two types of radial microcracks: Type I ($\sim$100 μm) with fracture surfaces perpendicular to the platelet faces and Type II (see arrows) parallel to the faces.

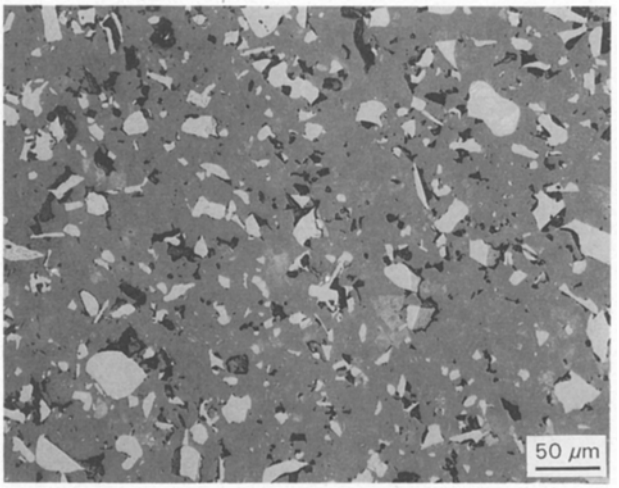

Figure 8 Optical micrograph shows that only Type II microcracks are present in a SiC platelet ($V = 0.2$)/Al_2O_3 composite using small size ($\sim$24 μm) platelets.

For platelet composites, reduction of platelet size first removes the Type I microcracks ($\sigma_{\alpha\alpha} < \sigma_{\theta\theta}$). The observed difference in crack length for Type I and II cracks in Fig. 7 is not clear. The shorter Type II cracks are expected because the highest stress is located at the interface of the inclusion and the matrix such that cracks tend to stay in the vicinity of the platelet edge rather than propagating away from it. In addition, the stresses are believed to drop greatly away from the interface. For example, Selsing showed that the radial and tangential stresses decreased to the third power with respect to the distance away from inclusions [28]. It is also expected that the shorter Type II microcracks are more favoured because this type of circumferential crack can relieve a larger fraction of the residual stresses by propagating around the platelet compared to Type I cracks. In order to determine the factors influencing the length of the Type I cracks, one would need to determine how $\sigma_{\alpha\alpha}$ changes with distance from the platelet.

The existence of spontaneous microcracking was also confirmed by the measurement of Young's modulus. Fig. 9 shows the Young's moduli of the composites as a function of SiC platelet volume fraction for two different directions: one parallel and the other perpendicular to the hot-pressing axis. It has been shown by Chou and Green [9] that there existed preferred platelet orientation in hot-pressed SiC platelet/Al_2O_3 composites with the faces of platelets lying

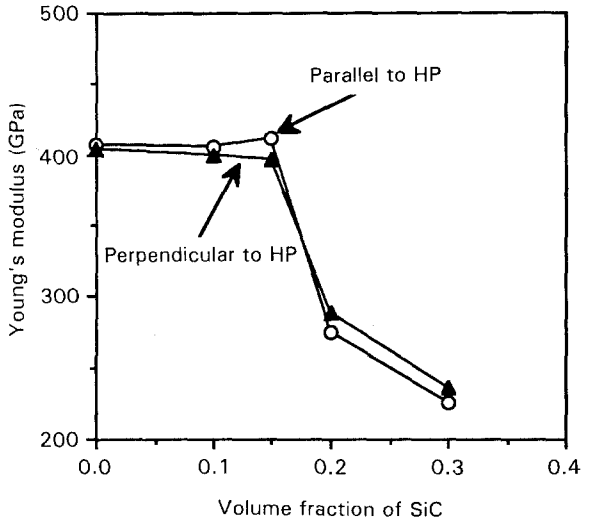

Figure 9 Young's modulus of the SiC platelet (~24 μm)/Al_2O_3 composites as a function of the SiC platelet volume fraction.

perpendicular to the hot-pressing axis. It is therefore appropriate to measure the Young's modulus along these two directions. From Fig. 9, it is clear that the moduli of composites show a slight increase or are unchanged with increasing SiC volume fractions up to $V = 0.15$. At higher volume fractions, the moduli drop abruptly for both directions, and this clearly indicates microcracks spontaneously forming as the material is cooled after fabrication.

It is interesting to note that the Young's modulus is greater in a direction parallel to the hot-pressing axis than the perpendicular direction at lower volume fractions ($V \leqslant 0.15$). The trend, however, reverses at higher volume fractions, i.e. the Young's modulus is greater in the perpendicular direction than the parallel direction. The phenomenon at lower volume fractions is not surprising because the Young's modulus of the SiC platelets is 510 and 455 GPa for parallel and perpendicular directions, respectively [29]. The decrease of the Young's modulus at high volume fractions for both directions is strictly due to the existence of spontaneous microcracking. Such a decrease should be a result of incomplete densification as the porosities of the composites are all less than 2%. Using various theories that consider the effect of porosity on the elastic constants, one can estimate that 2% porosity is unlikely to reduce the modulus by more than ~ 5%, unless it is in the form of microcracks. Similar behaviour has been observed in many ceramics, for example $MgTi_2O_5$ [30] and ZrO_2/Al_2O_3 [31] ceramics.

The trend that Young's modulus at higher SiC volume fractions is greater in the perpendicular direction than the parallel direction is most likely due to the morphologies of these microcracks. As mentioned in the previous section, Type II microcracks are likely to lie with crack planes parallel to the platelet faces due to the highest tensile stresses, $\sigma_{\theta\theta}$. Therefore, the Young's modulus of the composite would be smaller when measured perpendicular to the crack planes (or parallel to the hot-pressing axis as shown in Fig. 9). The effect of crack orientation on the reduction of Young's modulus has been analysed by Hasselman and Singh [32]. They predict that cracks with preferred orientation, for example, if the crack planes are parallel to each other, should result in lower Young's modulus when measured perpendicular to the crack planes compared to the parallel direction. Our results are consistent with their conclusions though the difference between the modulus for the two directions is not as substantial as suggested by their analysis for perfectly aligned cracks (note that the test method for Young's modulus, the ultrasonic velocity method, often yields precise measurements (error $\leqslant 1\%$), indicating that the measured difference along these two directions is not due to experimental error). The discrepancy is most likely due to the SiC platelets not being perfectly aligned parallel to each other and thus neither will the cracks. Nevertheless, the anisotropy in the Young's modulus of the microcracked composites clearly demonstrates the importance of the residual stress analysis in providing insight into the microcracking process. Finally, it has been shown that further reduction in platelet size to 12 μm can remove both types of microcracks [9]. Table III lists the Young's modulus of the composites with two different sizes of SiC platelets. It is clear that no reduction of Young's modulus is observed for composites using small-sized platelets. This is a critical step in producing brittle platelet composites with maximum strength and fracture toughness.

TABLE III Young's modulus of the composites along the hot-pressing direction for two different size of platelets

Platelet size (μm)	Young's modulus (GPa) for volume fractions of SiC:			
	0.0	0.1	0.2	0.3
24	407	405	275	225
12	403	411	415	419

6. Conclusions

The residual stresses associated with α-SiC platelets in a polycrystalline alumina matrix were determined. The results indicate that both the stresses inside and just outside the inclusion are dependent on the morphology (aspect ratio) and the volume fraction of SiC particles. However, the changes in stresses are limited for aspect ratios $\geqslant 10$. Owing to the anisotropy in the elastic and thermal expansion properties of α-SiC, two different tangential tensile stresses, $\sigma_{\theta\theta}$ and $\sigma_{\alpha\alpha}$, were evaluated. It is found that $\sigma_{\theta\theta}$ is much greater than $\sigma_{\alpha\alpha}$ at low angles ($\phi \leqslant 10°$), and they become equal at other angles ($\phi \geqslant 10°$). The tensile stresses are found responsible for the formation of spontaneous microcracking in a SiC platelet/Al_2O_3 composite. Microcracks with two different morphologies are found from optical microscopy and the measurement of the Young's modulus. The difference in morphology is consistent with the stress calculation. The analysis clearly demonstrates its importance in providing insight into the microcracking behaviour of ceramic platelet composites.

Acknowledgement

This work was supported by the Center for Advanced Materials, The Pennsylvania State University, University Park, PA 16802, USA.

References

1. G. C. WEI and P. F. BECHER, *Am. Ceram. Soc. Bull.* **64** (1985) 298.
2. P. F. BECHER and G. C. WEI, *J. Am. Ceram. Soc.* **67** (1984) C-267.
3. H-W LEE and M. D. SACKS, *ibid.* **73** (1990) 1884.
4. H. M. JANG, W. E. RHINE and H. K. BOWEN, *ibid.* **72** (1989) 948.
5. N. CLAUSSEN, in "11th RISO International Symposium on Metallurgy and Materials Science 1990", edited by J. J. Bentzen, J. B. Bilde-Sorensen, N. Christiansen, A. Horsewell and B. Ralph (Chapman and Hall, London, 1969) p. 1.
6. G. SANDERS and M. V. SWAIN, *Mater. Forum* **14** (1990) 60.
7. C. NISCHIK, M. M. SEIBOLD, N. A. TRAVILZKY and N. CLAUSSEN, *J. Am. Ceram. Soc.* **74** (1991) 2464.
8. W. B. JOHNSON, A. S. NAGELBERG and E. BREVAL, *ibid.* **74** (1991) 2903.
9. Y-S CHOU and D. J. GREEN, *ibid.*, submitted.
10. Z. LI and R. C. BRADT, *ibid.* **72** (1989) 70.
11. C-H HSEUH, *ibid.* **72** (1989) 344.
12. S. MAJUMDAR and D. KUPPERMAN, *ibid.* **72** (1989) 312.
13. A. ABUHASAN, C. BALASINGH and P. PREDECKI, *ibid.* **73** (1990) 2474.
14. S. MAJUMDAR, D. KUPPERMAN and J. SINGH, *ibid.* **71** (1988) 858.
15. Z. LI and R. C. BRADT, *Int J. High Tech. Ceram.* **4** (1988) 1.
16. *Idem, J. Mater. Sci.* **22** (1987) 2557.
17. *Idem, J. Am. Ceram. Soc.* **70** (1987) 445.
18. J. D. ESHELBY, *Proc. R. Soc. (Lond.) Ser. A* **241** (1957) 376.
19. T. MORI and K. TANAKA, *Acta Metall.* **21** (1973) 571.
20. T. MURA and P. C. CHENG, *ASME J. Appl. Mech.* **44** (1977) 591.
21. Z. LI and R. C. BRADT, *J. Am. Ceram. Soc.* **72** (1989) 459.
22. Z. LI, PhD thesis, University of Washington, Seattle, WA (1988).
23. W. E. TEFFT, *J. Res. NBS* **70A** (1966) 277.
24. J. B. WACHTMAN, JR, T. G. SCUDERI and G. W. CLEEK, *J. Am. Ceram. Soc.* **45** (1962) 319.
25. G. P. TANDON and G. J. WENG, *J. Appl. Mech.* **53** (1986) 511.
26. R. W. DAVIDGE and T. J. GREEN, *J. Mater. Sci.* **3** (1968) 629.
27. D. J. GREEN, in "Fracture Mechanics of Ceramics", Vol. 5, edited by R. C. Bradt, A. G. Evans, F. F. Lange and D. P. H. Hasselman (Plenum Press, New York, 1983) pp. 457–78.
28. J. SELSING, *J. Am. Ceram. Soc.* **44** (1961) 419.
29. Y-S CHOU, PhD thesis, The Pennsylvania State University (1992).
30. J. A. KUSZYK and R. C. BRADT, *J. Am. Ceram. Soc.* **56** (1973) 420.
31. D. R. CLARKE and D. J. GREEN, in "Advances in Materials Characterization", edited by D. R. Rossington, R. A. Condrate and R. I. Snyder (Plenum, New York, 1983) p. 323.
32. D. P. H. HASSELMAN and J. O. SINGH, *Am. Ceram. Soc. Bull.* **58** (1979) 856.

Received 10 March 1993
and accepted 16 May 1994